HEAT TREATMENT INFLUENCE ON STRUCTURE AND PROPERTIES OF SOME NEW Ni-BASED SUPERALLOYS

George COMAN[1], Andrei Constantin BERBECARU[1,*], Andrei GRECU[1], Mirela SOHACIU[1], Ecaterina MATEI[1], Andra Mihaela PREDESCU[1], Ruxandra Elena DUMITRESCU[1], Ioana Arina GHERGHESCU[1], Ionela Alina DIACONU[1], Elena MARGHIOALA[1],Sorin CIUCĂ[1], Cristian PREDESCU[1]

The paper presents the influence of solution treatment and two-stage aging on the microstructure and properties (corrosion resistance in sulfuric acid solution and hardness) of some experimental Ni-based superalloys with different Re additions of 1.96%, 2.98% and 1.02%, respectively. After aging, the hardness of the three solution treated alloys slightly increased because of the increasing Re content. Nevertheless, the hardness values are similar. Also, the behaviour in corrosive environments of the three solution treated and aged alloys is similar. One can mention that the sample with 2.98% Re shows a slightly higher corrosion resistance.

Keywords: Ni based superalloys, age hardening, solution treatment, two-stage aging, corrosion resistance, rhenium

1. Introduction

Characterized by superior mechanical strength properties at high temperatures, above 750 °C, and corrosion resistance in various environments, Ni-based superalloys have wide applicability in fields such as aeronautics, aerospace, mining, energy field, etc. [1-3].

The excellent mechanical properties are mainly due to two hardening mechanisms: solute hardening and precipitation hardening. While the former is found in all superalloys, the latter is conditioned by a certain chemical composition that determines the formation of the γ′ and γ″ phases. Subsequently, the aging heat treatment applied after the solution treatment favors the precipitation/reprecipitation of these toughening phases, that are coherent with the γ matrix.

By choosing the optimal heat treatment parameters, significant increases in hardness, but also in yield strength, tensile strength, etc. can be achieved.

Thus, Fumitaka Ichikawa et al. observed a hardness sharp increase of a Ni-Fe-Cr-Ti-Nb-Mo superalloy with increasing aging holding time in the range of

[1] Faculty of Materials Science and Engineering, National University of Science and Technology POLITEHNICA Bucharest, Romania
* Corresponding author's e-mail: andrei.berbecaru@upb.ro

0.03-3 h [4]. The extension of the holding time determined a hardness decrease from the maximum value of 536 HV to 437 HV, the latter being recorded after 400 h of aging [4].

Then again, in the case of some single crystal Ni-based superalloys, Shunyong Zhang et al. noted a continuous increase in hardness when prolonging the aging holding time [5].In this study, the hardness of the superalloy with a 30% hardening phase proportion increases continuously from approximately 4.7 GPa (initial hardness) to 5.8 GPa - a value reached after 1000 h of holding time. At the same time, it was found that elastic modulus shows very small variations with the aging holding time [5]. Relatively common, two-stage aging is applied to Ni-based superalloys, which contain both γ′ and γ″, in order to favor precipitation and increase the number of hardening phases [6, 7].

Another type of heat treatment was proposed by Fencheng Liu et al., a treatment that involves aging at a high temperature of 890 °C, the so-called δ aging, which favors the δ phase precipitation. By stimulating its formation, the morphology of the Laves phase is modified, with beneficial effects on the mechanical properties [2]. Thus, one can see that heat treatments have a major influence on the precipitation hardened Ni-based superalloys properties. In the present paper the experimental compositions of modified Inconels with Re additions, proposed by the authors in a previous paper [8], are subjected to solution treatment and two-stage aging heat treatments. The heat treatments effects on the superalloy smicrostructures and properties (hardness and corrosion resistance) are studied.

2. Materials and Methods

Further research on thethree Ni-based superalloys with different rhenium proportions: 1, 2, and 3%, respectively [8], was done. The materials were obtained in a Five CELES induction furnace (model ALU 600), in vacuum. During casting, the melt was protected by a controlled argon atmosphere. The chemical composition of the superalloys, determined with the Leco GDS 500 A optical emission spectrometer, is shown in Table 1[8].

Table 1

Chemical composition of the three Ni-based superalloys (wt%) [8]

Alloy/ Sample code	Al (%)	Mo (%)	Cr (%)	Ni (%)	Ti (%)	Fe (%)	Nb (%)	Ta (%)	W (%)	Re (%)	C (%)	Co (%)
Alloy 1/S1	5.20	0.58	6.92	63.04	1.49	-	-	6.58	4.34	1.96	0.02	9.87
Alloy 2/S2	8.27	0.56	6.47	60.06	1.45	-	-	6.27	4.31	2.98	0.02	9.61
Alloy 3/S3	5.43	2.71	12.62	64.28	0.79	1.76	0.76	3.38	1.28	1.02	0.03	5.89

The three cast samples were subjected to homogenizing annealing at 1200 ºC for 8 h holding time and subsequently solution treatment followed by aging. The heat treatments were applied in a chamber - like laboratory furnace, heated with electrical resistances and having a maximum temperature T = 1400 °C.

The parameters of the secondary heat treatments applied to the superalloys are shown in Table 2.

Table 2

Heat treatment parameters applied to S1-S3 alloys

Heat treatment	Heat treatment temperature [ºC]	Holding time [h]	Cooling rate [°C/min] or cooling medium
Solution treatment	1000	1	water
Two-stage aging	720/620	8/8	5 (down to 620 °C) /air

Microscopic analysis was performed after each heat treatment (solution treatment/aging) using a QUANTA 450 FEG scanning electron microscope.Energy dispersive X-ray microanalyses were also performed.

The Vickers hardness HV2 was determined using an Innovatest Falcon 500 automatic hardness testing machine. Such measurements were done for each sample, after quenching and aging.

The corrosion behavior in sulfuric acid puriss. p.a., 0.1N at 25 ºC of the solution treated and aged samples was evaluated using a three-electrode electrochemical cell with platinum counter electrode and Ag/AgCl 3M reference electrode, Gamry Reference 300 potentiostat/galvanostat.

3. Results and discussion

3.1. Microstructural and compositional analysis

Fig. 1 shows the microstructure of the solution treated S1 sample, with a selection of an area (Fig. 1*b*) where the chemical composition was determined by X-ray (Fig. 2).

The structure obtained after solution treatment is biphasic, γ + γ′. The chemical analysis in the selected area (Fig. 2) indicates that the cuboidal particles belong to the γ′ – Ni_3(Cr, Al) phase. The calculations that allowed this statement refer to the ratio of atomic percentages between Ni, Cr and Al, meaning $\frac{\%at\ Ni}{\%at\ Cr+\%at\ Al} = \frac{66.07}{15,18+6.11} = 3.103 \sim 3$, so the compound has the formula Ni_3(Cr, Al).

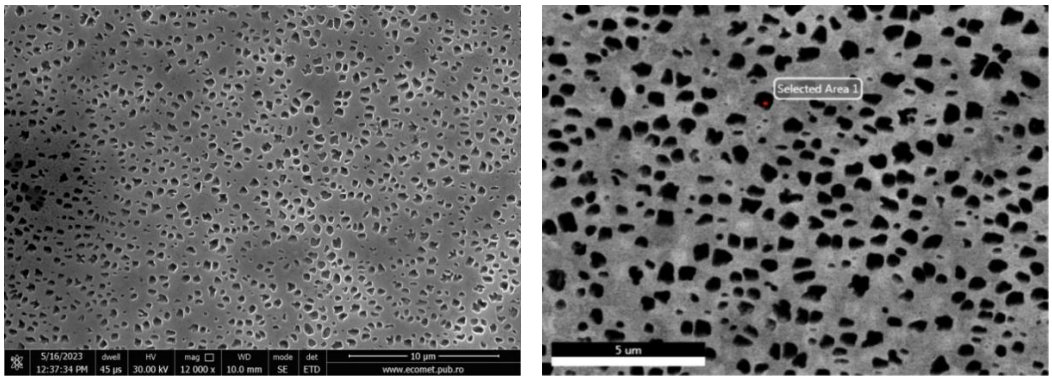

a) b)

Fig. 1. Scanning electron microscopy (SEM) image of S1 - solution treatedsample; a. Secondary electrons image; b. Backscattered electrons image with the specification of the area where the EDS compositional analysis was performed

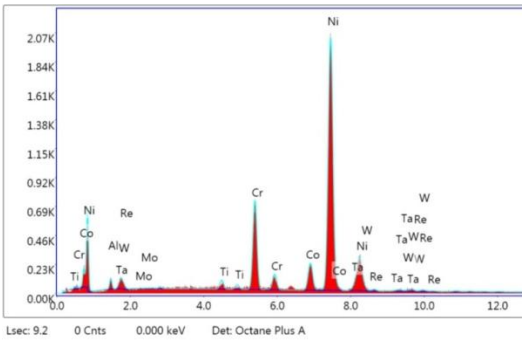

Element	Weight %	Atomic %
AlK	2.75	6.11
TiK	1.19	1.49
CrK	13.16	15.18
CoK	6.09	6.20
NiK	64.70	66.07
TaL	4.59	1.52
W L	2.81	0.92
ReL	1.43	0.46
MoK	3.28	2.05

Fig. 2. Energy-dispersive X-ray spectrum for the selected microarea of the S1- solution treated sample, with specification of the quantitative chemical composition

One may see that the polyhedral shapes of the γ′ phase found in the S1 sample - solution treated - have rounded corners, furthermore in certain microregions the "erosion" of the edges makes the particles have a quasi-globular appearance. The morphological changes are an effect of the heat treatment which acted on the tendency of the γ′ phase to dissolve by solubilizing itself in the neighboring γ solid solution.

Figs. 3 and 4 show the microstructure, respectively the chemical composition of an area of the solution treated S2 sample. In Figs. 3 *a* and 3 *b* both the secondary electrons and backscattered electrons images highlight a dark, majoritary area belonging to the γ′ phase (in accordance with its morphology), and a bright, network-like area, specific to the minoritary γ solid solution.

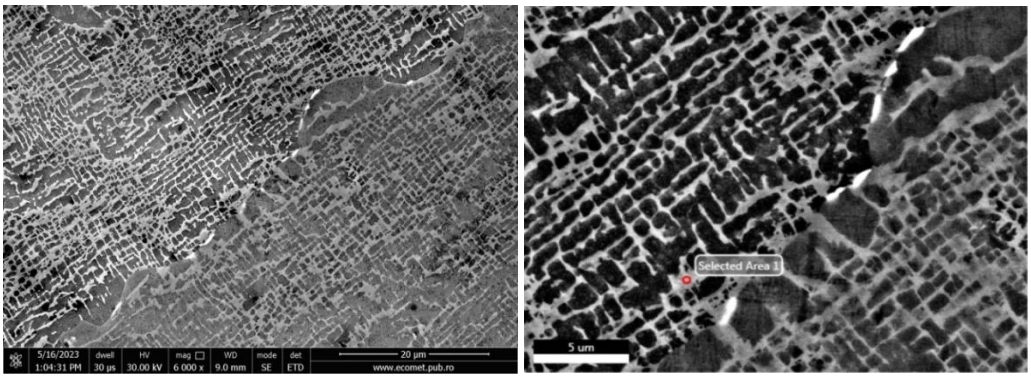

a) b)

Fig. 3. Scanning electron microscopy (SEM) image of S2 - solution treated sample; a. Secondary electrons image; b. Backscattered electrons image with the specification of the area where the EDS compositional analysis was performed

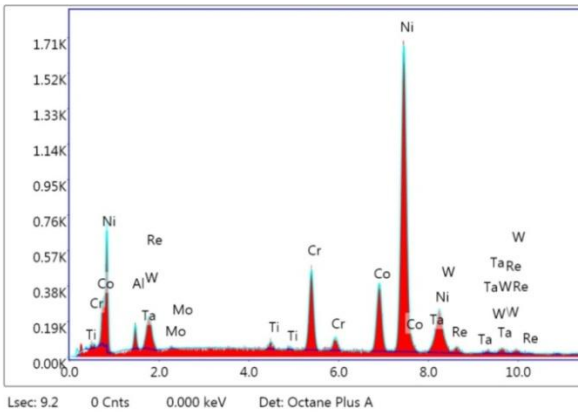

Element	Weight %	Atomic %
AlK	4.71	10.69
TiK	0.79	1.01
CrK	8.78	10.33
CoK	11.21	11.63
NiK	56.92	59.31
TaL	4.71	1.59
W L	5.34	1.78
ReL	3.72	1.22
MoK	3.82	2.43

Fig. 4. Energy-dispersive X-ray spectrum for the selected microarea of the S2- solution treated sample, with specification of the quantitative chemical composition

The chemical composition (Fig. 4) of the selected area (Fig. 3 *b*) indicates that it belongs to the γ phase (distributed as a network), having elements contents that are preferentially distributed in the solid solution above the alloy average (Cr, Co, Re, Mo, W) concentrations [9-13].

In micrographs 5 *a* and *b* of sample S3 subjected to solution treatment, the secondary electrons and backscattered electrons images capture a predominantly biphasic structure similar to that of S2sample, consisting of γ solid solution (bright, lattice-like areas) and γ′ phase (dark areas).

To determine the local chemical composition, a microvolume (Fig. 5 *b*) was selected from the γ solid solution filamentary network, the results being presented in Fig. 6.

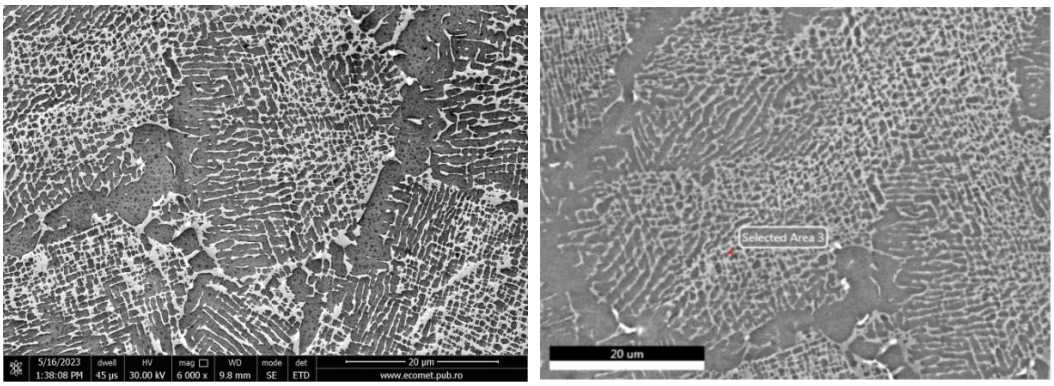

Fig. 5. Scanning electron microscopy (SEM) image of S3 - solution treated sample; a. Secondary electrons image; b. Backscattered electrons image with the specification of the area where the EDS compositional analysis was performed.

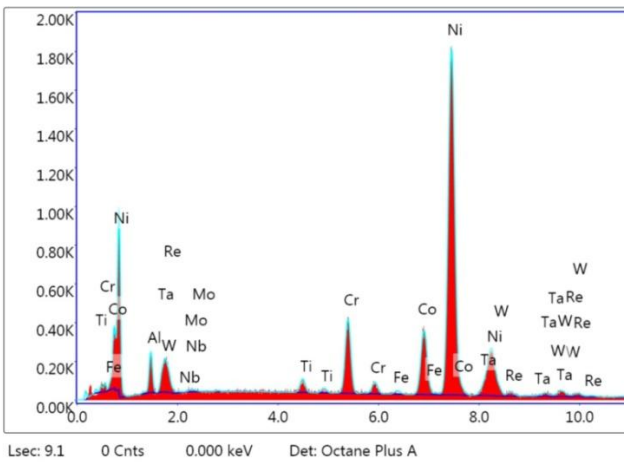

Element	Weight %	Atomic %
AlK	6.06	13.50
TiK	1.15	1.45
CrK	7.24	8.37
FeK	0.36	0.39
CoK	9.38	9.56
NiK	57.74	59.11
TaL	5.44	1.81
W L	4.72	1.54
ReL	2.41	0.78
NbK	2.50	1.62
MoK	2.99	1.87

Fig. 6. Energy-dispersive X-ray spectrum for the selected microarea of the S3- solution treated sample, with specification of the quantitative chemical composition

Unlike the γ phase in the S2 sample microstructure, enriched only in elements that are preferentially distributed in the disordered solid solution, in the γ matrix of sample S3 a significant increase in the concentration of all elements (except Cr and Fe – possibly found mainly in TCP phases) is observed, when compared to the average chemical composition of the alloy. This suggests a more pronounced supersaturation of the sample S3 alloy matrix compared to that of sample S2, respectively a superior effect of solution treatment on sample S3. A possible explanation may be the lower Re content in S3. Re is characterized by the lowest diffusion coefficient among all alloying elements in Ni-based

superalloys [14-16]. Thus, it determines an overall reduction in the diffusion rate, the more drastic the higher its concentration.

As expected, in the γ phase of both samples the Re content is considerably higher when compared to the chemical composition of the alloys (3.72 vs. 2.98% in S2 and 2.41 vs. 1.02% in S3). This confirms once again that in Ni-based superalloys, Re is preferentially dissolved in the disordered solid solution, probably forming clusters in the matrix that prevent dislocation movement, with beneficial effects on hardness [17].

Figs. 7*a* and 7 *b* show the micrographs of the solution treated and aged S1 sample, respectively the EDS analysis of the selected area in Fig. 7*b* is shown in Fig. 8.

As already seen in S1 solution treated sample, the majoritary structure is formed by the brighter background - γ solid solution and the cuboidal shapes - γ′ phase. On the surface of the γ matrix, as against to that seen in Fig. 1, a fine arrangement of precipitates resulted from artificial aging is observed. In addition to the two phases mentioned above, some discontinuous white coloured precipitates scattered in the solid solution matrix are also to be seen in Figs. 7 *a* and 7 *b*.

The local chemical composition analysis (Fig. 8) made right in the center of such a particle (Fig. 7 *b*) identifies a significant amount of carbon. Thus, it can be stated that the white particles are carbides. These are part of the secondary carbides that followed the transformation path MC (primary carbide) → $M_{23}C_6$ or MC → M_6C facilitated by the heat treatment temperature T_{HT}=720°C from the first aging stage. One may see some bigger carbides arrangement at the grain boundaries. They generate a barrier effect on the dislocation displacement, therefore leading to an improvement in creep behavior.

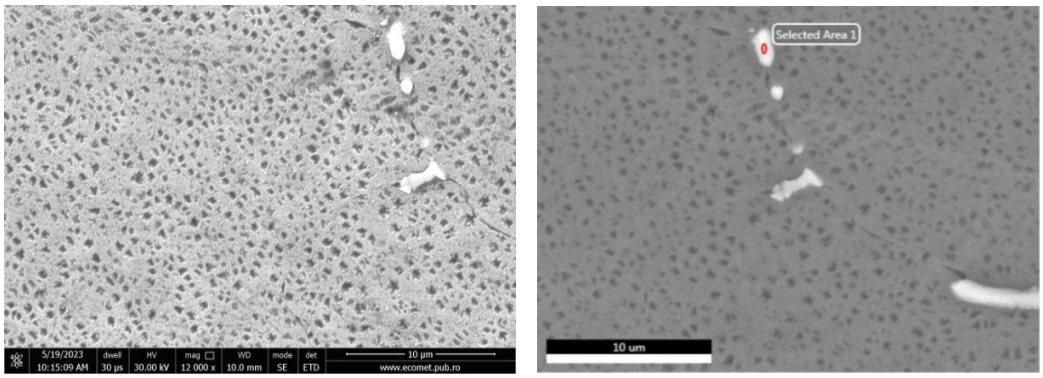

a) b)

Fig. 7. Scanning electron microscopy (SEM) image of S1 - solution treated + aged sample; a. Secondary electrons image; b. Backscattered electrons image with the specification of the area where the EDS compositional analysis was performed

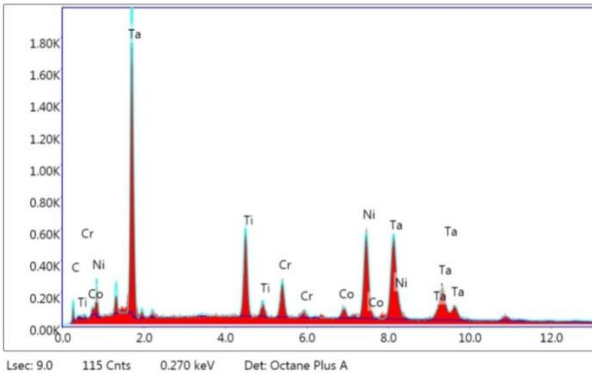

Element	Weight %	Atomic %
C K	12.62	31.81
TiK	11.77	12.12
CrK	5.59	5.30
CoK	2.13	1.78
NiK	18.51	15.54
TaL	49.37	33.45

Fig. 8. Energy-dispersive X-ray spectrum for the selected micro area of the S1 - solution treated+ aged sample, with specification of the quantitative chemical composition

Fig. 9 shows the microstructure of the solution treated and aged S2 sample. One may note that it is mainly composed of two phases: the γ solid solution and the γ′ phase. The latter is majoritary, cuboidal in shape, dark coloured, while the γ solid solution is distributed as a bright lattice.

The chemical elements concentration values in the γ phase after aging (Fig. 10) are generally close to those obtained after solution treatment (Fig. 4). One may note the following differences: the decrease in the Al proportion (γ′ phase former), as a result of aging precipitation and the significant increase in Mo, an element that preferentially dissolves in the γ phase.

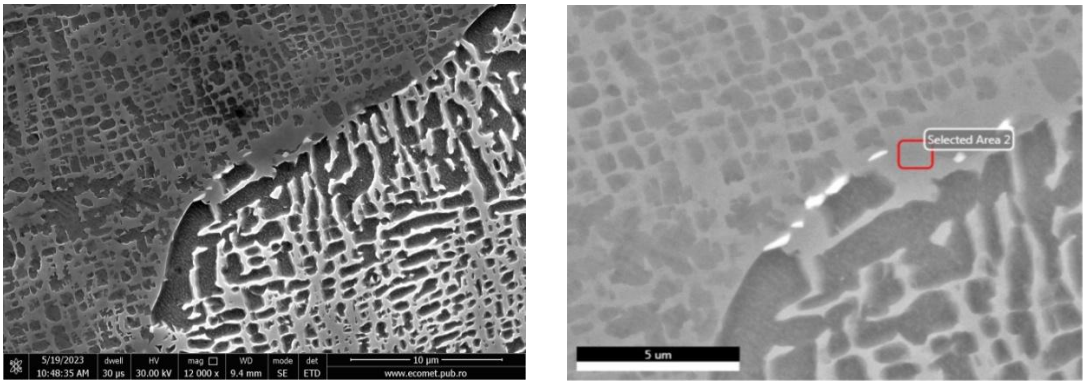

a) b)

Fig. 9. Scanning electron microscopy (SEM) image of S2 - solution treated + aged sample; a. Secondary electrons image; b. Backscattered electrons image with the specification of the area where the EDS compositional analysis was performed

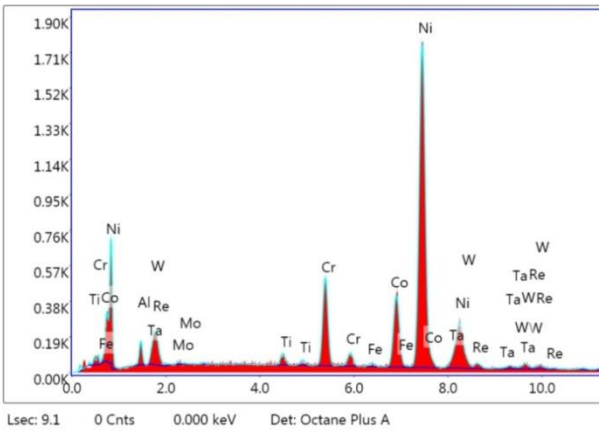

Element	Weight %	Atomic %
AlK	4.10	9.35
TiK	1.06	1.36
CrK	9.02	10.66
FeK	0.44	0.48
CoK	11.11	11.59
NiK	56.48	59.14
TaL	4.96	1.68
W L	5.16	1.72
ReL	2.94	0.97
MoK	4.73	3.03

Fig. 10. Energy-dispersive X-ray spectrum for the selected microarea of the S2 - solution treated+ aged sample, with specification of the quantitative chemical composition

White particles with a lenticular shape are also observed (Fig. 9 and 11 *a*), precipitated both inside the γ matrix and in the immediate vicinity of the γ/γ′ interface. Considering the morphology and arrangement of this phase and correlating with the EDS analysis (Fig. 11 *b*) it can be stated that the white particles belong to TCP phases (topological close packed phases), most likely Laves phases, whose generation is favored by elements such as Re (sample S2 has the highest content of all the studied alloys), but also other refractory elements such as W and Mo [18, 19].

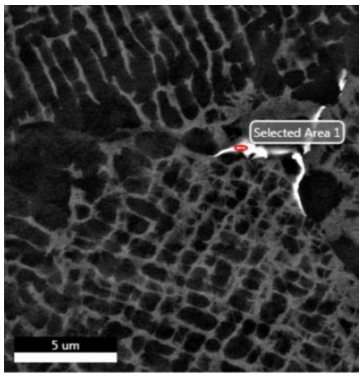

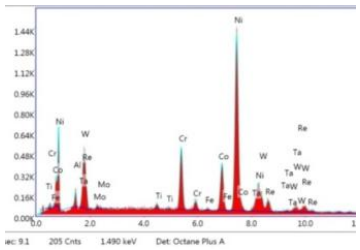

Element	Weight %	Atomic%
AlK	3.82	9.53
TiK	0.86	1.20
CrK	9.95	12.88
FeK	0.37	0.45
CoK	10.66	12.17
NiK	44.93	51.51
TaL	3.59	1.34
W L	11.63	4.26
ReL	9.73	3.52
MoK	4.47	3.13

a) b)

Fig. 11. a) Scanning electron microscopy (SEM) image of S2 - solution treated + aged sample exhibiting a filiform, white phase; b) Energy-dispersive X-ray spectrum for the new selected microarea of the S2 - solution treated+ aged sample, with specification of the quantitative chemical composition

Indeed, the following metals fulfill the Laves phases formation conditions [20]:

Co - r_{Co}=1.26 Å, Ta - r_{Ta} =1.70 Å and W - r_W =1.62 Å, where r = atomic radius, Å (Goldschmidt radius). In order to have a Laves phase formation, it is necessary that $\frac{rA}{rB}$~1.225:

$$\frac{(r_{Ta}+r_W)/2}{r_{Co}} = \frac{(1.70+1.62)/2}{1.26} = \sim 1.31, \text{ value close to } 1.225$$

Regarding Ta and W, the average atomic radius was considered, without making a very strict calculation on the participation of each element in the chemical composition. Therefore, the analyzed Laves phase can be considered (Fig. 11 *b*) with the following components:

$$\frac{\%at\ Co}{\%at\ (Ta+W)} = \frac{12.17}{1.34+4.26} = 2.17 \sim 2$$

In conclusion, the Laves phase, present in the S2 alloy, may have the chemical formula $Co_2(Ta,W)$.

In Figs. 12 and 13 are presented the micrographs of the solution treated and aged S3 sample and, respectively, the EDS analysis of the selected area seen in Fig. 12 b.

The electron micrographs are similar to those in the solution treated state, showing a mostly biphasic structure, with the majoritary γ′ phase (dark background of the image) and the minoritary γ solid solution, in the form of a luminous network. White particles with a morphology similar to those in the micrographs in Figs. 9 and 11 can also be observed and are therefore attributed to Laves phases.

The chemical analysis performed in a dark area (Fig. 12 *b* and Fig. 13) attests that the studied micro area belongs to the γ′ phase. Since the ratio of the atomic concentrations of the elements Ni, Cr and Al is:

$$\frac{\%at\ Ni}{\%at\ (Cr+Al)} = \frac{62.82}{3.73+16.77} = 3.06 \sim 3$$

the γ′ - based intermetallic compound is again confirmed to be $Ni_3(Cr, Al)$.

The luminous γ solid solution lattice (Fig. 12 *a*) presents on its surface a very fine, submicron size dispersion of particles, light-gray shaded.

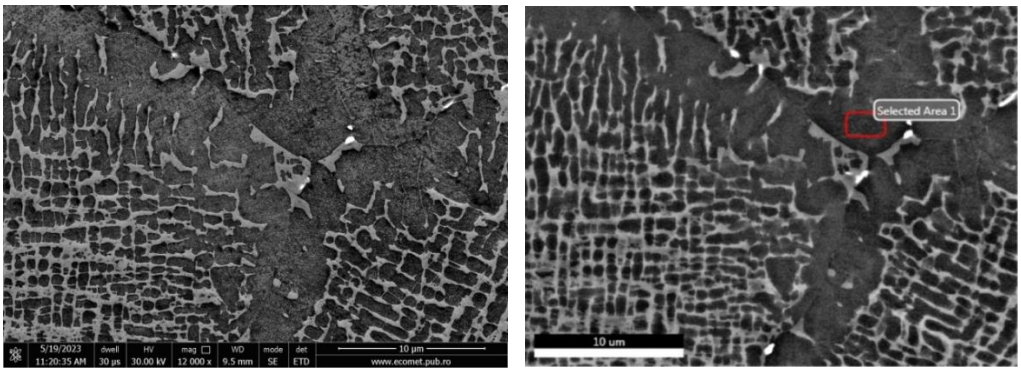

Fig. 12. Scanning electron microscopy (SEM) image of S3-solution treated + aged sample; a. Secondary electrons image; b. Backscattered electrons image with the specification of the area where the EDS compositional analysis was performed.

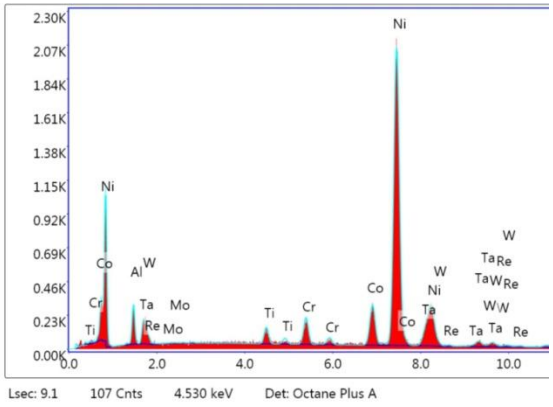

Element	Weight %	Atomic %
AlK	7.59	16.77
TiK	1.83	2.28
CrK	3.25	3.73
CoK	7.10	7.18
NiK	61.88	62.82
TaL	10.30	3.39
W L	3.02	0.98
ReL	0.88	0.28
MoK	4.15	2.58

Fig. 13. Energy-dispersive X-ray spectrum for the selected microarea of the S3 - solution treated+ aged sample, seen in Fig. 12 b, with specification of the quantitative chemical composition

Among them, those having an island-like arrangement indicate a possible association with the γ phase, and those exhibiting an acicular shape, with the δ phase. In the backscattered electron image of sample S3 -solution treated+ aged (Fig. 14 a) - the zone of the γ solid solution network where acicular particles can be observed was selected for chemical analysis.

Analyzing the chemical composition values (Fig. 14 b), a higher concentration of Nb is found, when comparing to the overall chemical composition of the alloy (2.58 wt% Nb - the analyzed portion - vs. 0.76 wt% Nb - the chemical composition of the S3 alloy). The increase in the Nb concentration suggests that the acicular particle belongs to the δ phase, because Nb stimulates its formation [21]. Computing the ratio of the atomic percentages of Ni, Cr, Al and Nb in this case as well, the result is:

$$\frac{\%\ Ni}{\%Cr+\%Al+\%Nb} = \frac{58{,}18}{8.75+11.42+1.72} = 2.65 \sim 3$$

Therefore, the δ phase is also based on the intermetallic compound $Ni_3(Cr,Al,Nb)$, according to [2] and [21].

Another important aspect related to the S3 sample structure is represented by the bright, dispersed particles, which belong to the Laves phases. Stimulating the precipitation of the δ phase upon aging brings benefits by shattering and dispersing this particularly dangerous phase.

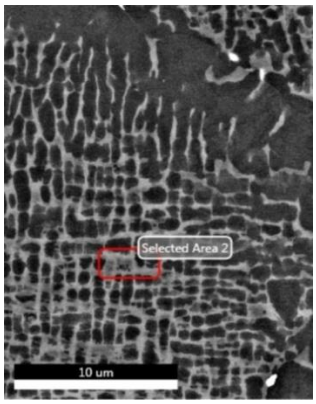

a)

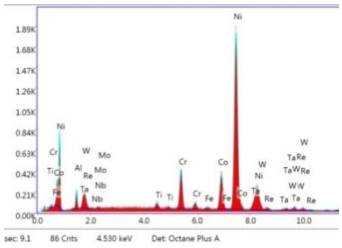

b)

Element	Weight %	Atomic %
AlK	4.98	11.42
TiK	1.13	1.45
CrK	7.36	8.75
FeK	0.60	0.66
CoK	9.63	10.11
NiK	55.21	58.18
TaL	6.19	2.12
W L	4.80	1.62
ReL	2.81	0.93
NbK	2.58	1.72
MoK	4.70	3.03

Fig. 14. a) Backscattered electron image of sample S3 - solution treated +aging showing the selected area where EDS compositional analysis was performed; b) Energy-dispersive X-ray spectrum for the selected microarea of the S3 - solution treated+ aged sample, seen in Fig. 14 a, with specification of the quantitative chemical composition

3.2. Effect of secondary heat treatments on materials hardness

The hardness values determined for each of the three samples after solution treatement and aging, respectively, are summarized in Table 3.

Table3

Samples S1, S2 and S3 hardness values determined after solution treatement and, respectively, after aging

Sample	Average hardness, HV2	
	After solution treatment	After aging
S1	259	372
S2	347	374
S3	347	370

As expected, aging led in all cases to an increase in hardness values after solution treatment, thus to an increase in mechanical strength performances.

The hardness increase was achieved in a uniform manner in each sample. The values were within the hardness intervals found in other research studies [2, 21- 23].

Furthermore, the alloys hardness after aging is approximately equal (≈370 HV), although the S3 alloy has the lowest content of alloying elements (economical variant, with the lowest Re proportion), of 35.72%, over 1.2%, respectively 4.2% lower than the other alloys.

3.3. Corrosion resistance evaluation of alloys S1-S3

The evaluation of the corrosion behavior of nickel alloys in 0.1N sulfuric acid solution at 25 °C was carried out using the following techniques:

1. Monitoring the evolution of the stationary potential for 60 minutes;
2. Polarization curve method drawn in the potential range -500mV to 1V at a speed of 2.5 mV/sec.
3. Tafel curve method in the range ± 250 mV/OPC at a speed of 2.5 mV/sec.

3.3.1. Variation of stationary potential over time

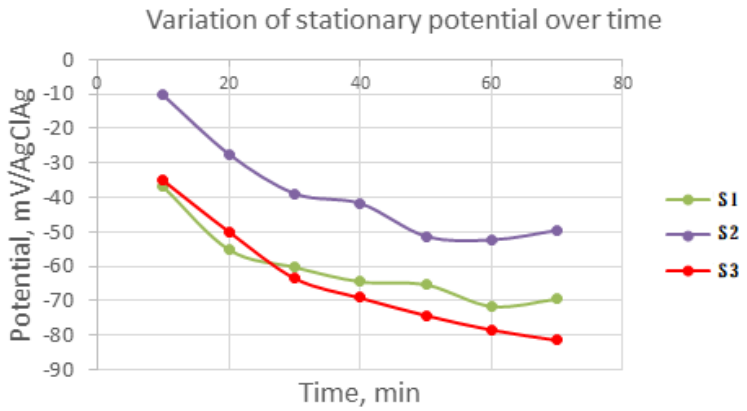

Fig. 15.Variation of stationary potential over timefor S1-S3samples

In Fig. 15 a similar variation of the three alloys stationary potentials is observed, the curves being relatively parallel. All samples have a normal variation of OCP negativity due to the dissolution of the native passivation film formed on the surface.Thus, no fundamental differences between the materials are found. OCP falls within the 100mV range. However, the alloys can be grouped into two categories with practically identical behaviors, namely S1-S3 and S2. The latter

has the most electropositive potential, with an obvious tendency to shift towards electropositive values, which means that aluminum has compensated for the decrease in chromium concentration with regard to the passivation capacity of the material.

3.3.2. Anodic polarization

The anodic polarization curves have the classic form of Ni-Cr alloys with potential ranges according to Fig. 16. The cathodic branch represents the hydrogen evolution range, and the anodic branch represents the oxidation range, the active range, the passive range and the transpassive range. A very wide active dissolution range specific to nickel and its alloys is observed, characterized by the presence of several secondary peaks, each specific to dissolution reactions of the alloys phases. The curves have approximately the same shape, which indicates similar compositions, but shifted relatively to each other as a result of some particularities of these chemical compositions. The main reaction that takes place in the potential range from -200 to -100mV is that of nickel oxidation:

$$Ni = Ni^{+2} + 2e^{-}$$

as well as other alloying elements with similar potentials, such as Mo. The formation of the various oxides takes place, then their redissolution and eventually the passivation film formation. The presence of very well-marked peaks in alloys S1-S3 may be evidence of the existence of well-individualized phases of the various alloying elements.

The presence of the two peaks at approximately -200mV and +100mV (Fig. 16) is the result of the metals dissolution and the formation of the superficial passive film. The peak at +250mV (Fig. 16) can be attributed to the metal carbides dissolution in NiCr alloys.

As a conclusion S3 is more difficult to passivate compared to the others, but the currents in the passive state are relatively small, between 100 and 350mA.cm^{-2}.

• The critical currents are relatively high (between 100 and 300 μA.cm^{-2}) but are 100 times lower than those of pure nickel for which the order of magnitude of the critical current is 300mA.cm^{-2};

• The most negative corrosion potentials, respectively the widest passivity range are found for S1 and S3;

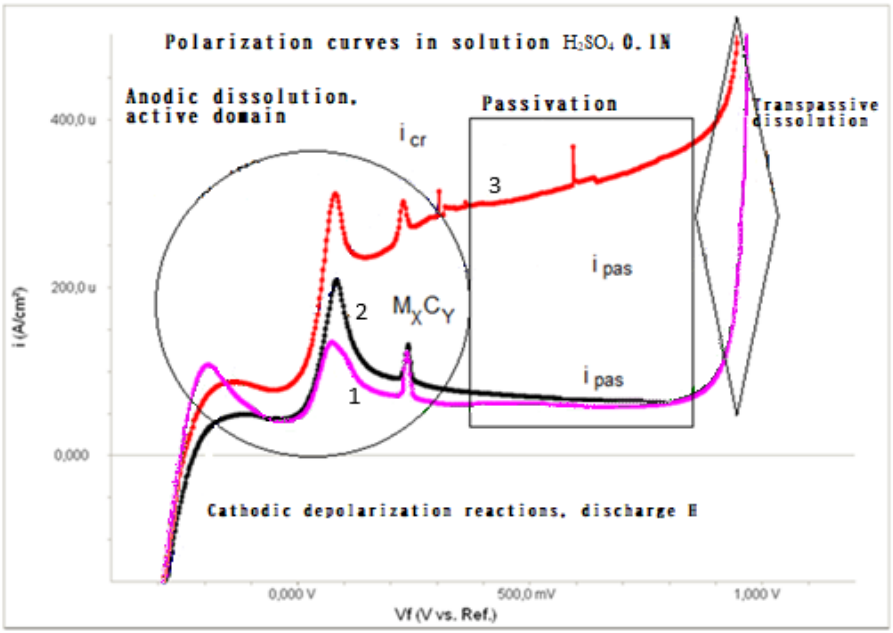

Fig. 16. Polarization curves for superalloys S1-S3

One should observe that all samples present the same value for the transpassive potential.

3.3.3. Tafel curves method used for corrosion rate evaluation

The Tafel curves are presented in Fig. 17, and the values of the corrosion parameters in Table 4.

Table 4

Corrosion parameters of S1-S3 alloys

Alloy	β_a, mV/decade	β_c, mV/decade	I_{corr}, µA/cm^2 (I)	E_{corr}, mV (V_f)
S1	1 e15	6.42e-2	59.4	-251
S2	1 e15	9.2e-2	51.4	-224
S3	1 e15	8.9e-2	54.5	-231

From the Tafel curves and the corrosion parameters analysis, the following aspects emerge:

- all curves have very high anodic slopes, which indicates the tendency of the alloys to passivate;
- the corrosion potentials of the S1-S3 alloys are very close in value, with differences of a few tens of mV;

- the lowest corrosion current density is for S2, but very close to S3.- in terms of corrosion resistance, there are no significant differences between the S1-S3 alloys.

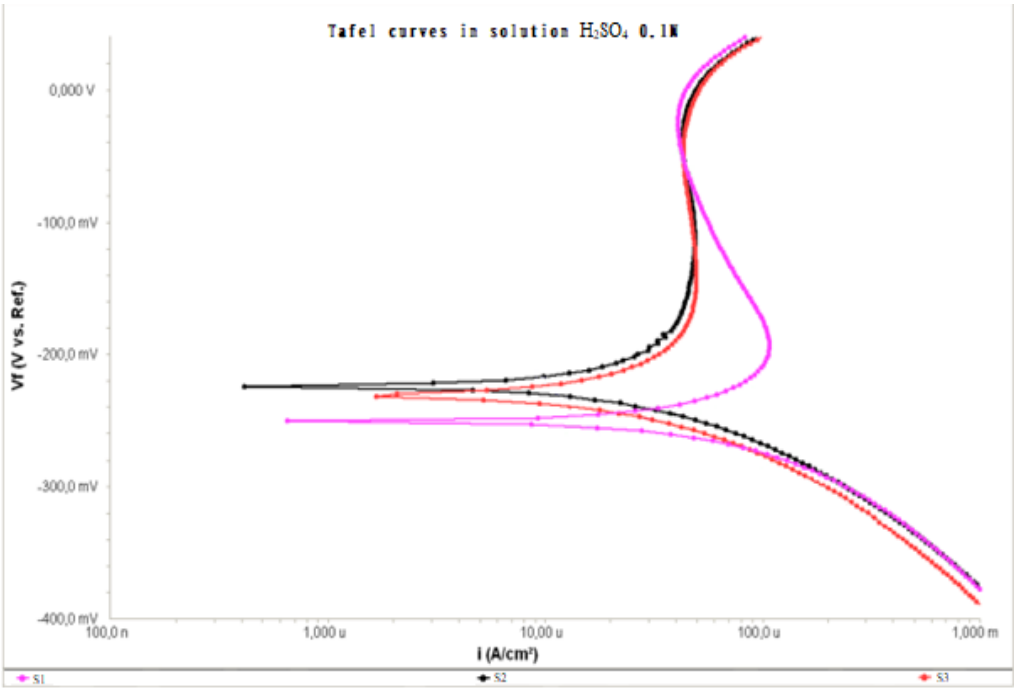

Fig.17. Tafel curves for evaluating the corrosion rate of samples S1-S3

4. Conclusions

- Structure and mechanical properties changes of the Ni-based superalloys studied in this work was possible by applying the *solution treatment* and *aging* heat treatments.
- The microstructure of S1-S3 alloys after applying the heat treatments is composed of γ solid solution (matrix), γ′ precipitates, carbides and TCP phases, most likely Laves phases.
- Controlled precipitation during aging for T_{HT}=720 ºC of the δ phase (sample S3) becomes the only possibility to mitigate the negative effects of the Laves phases. From the point of view of the acicular morphology, the δ phase does not have a complete hardening effect, inducing to some extent brittleness and an inadequate creep behavior. Its controlled precipitation at T_{HT}=720 ºC allows it to appear only in the neededamount for mitigating the effects of the Laves phases.

- The precipitation of the main hardening phase, the γ′ phase, is carried out at lower temperatures, namely at T_{HT} =620 ºC.
- The application of two-stage aging had the following objectives: controlled precipitation of the δ phase and ensuring appropriate hardness through the precipitation of the main hardening phase γ′.
- The alloys hardness after aging is approximately the same, with differences of a few Vickers units; however, a slight increase in this characteristic is noted with increasing Re content.
- Regarding the corrosion resistance obtained after aging, it also does not show any notable differences from one alloy to another; one may mention that S2 alloy, having the highest Re content, has the lowest corrosion current density and the highest value for the corrosion potential. However, a direct correlation cannot be established only between the Re content and the alloys corrosion resistance, since the second best corrosion behavior after sample S2 is that of sample S3, having the lowest Re content of all three studied alloys.
- Considering the very close mechanical and chemical resistance characteristics of the three alloys, one will consider that the optimal alloy from the properties point of view is the one with the most "economical" chemical composition, namely the one with the lowest Re proportion (Re being an element with a particularly high price) - S3.

R E F E R E N C E S

[1] *D. Liu, Q. Ding, Q. Zhou, D. Zhou, X. Wei, X. Zhao, Z. Zhang, H. Bei*, Microstructure, Mechanical Properties and Thermal Stability of Ni-Based Single Crystal Superalloys with Low Specific Weight, Crystals, Vol. **13**, Iss. 4, 2023.

[2] *F. Liu, F. Lyu, F. Liu, X. Lin, C. Huang*, Laves phase control of Inconel 718 superalloy fabricated by laser direct energy deposition via δ aging and solution treatment, J. Mater. Res. Technol., Vol. **9**, Iss. 5, 2020.

[3] *A. Kracke*, Superalloys, the Most Successful Alloy System of Modern Times-Past, Present, and Future. DOI: 10.1002/9781118495223.ch2, in book: Superalloy 718 and Derivatives, 2012

[4] *F. Ichikawa, M. Sawada, Y. Kohigashi*, Age-hardening Behavior in *γ′*-phase Precipitation-hardening Ni-based Superalloy, ISIJ International, Vol. **63**, Iss. 6, 2023.

[5] *S. Zhang, B. Zhang, F. Zhao, J. Li, L. Wei, X. Huang*, (2024). Influence of Aging Treatment and Volume Fraction on Nano-Indentation Behavior of Ni-Based Single Crystal Superalloys. *Materials*, Vol. **17**, Iss.24, 2024.

[6] T. Homma, K. Katayama, M. Okuno, D. Nagahama, Effects of microstructures and double aging on high temperature yield strength in Ni-Co-base superalloy produced by a powder metallurgy route, Intermetallics, Vol. **174**, 2024.

[7] *C. Slama, C. Servant, G. Cizeron*, Aging of the Inconel 718 alloy between 500 and 750 °C, J. Mater. Res., Vol. **12**, Iss. 9, 1997.

[8] *A.C. Berbecaru, G. Coman, S. Ciucă, A. Grecu, I.A. Gherghescu, M. Dobre, M. Sohaciu, E. Matei, A.M. Predescu, I.A. Diaconu, C. Predescu*, Characterization of some rhenium inconel superalloys made in a vacuum induction furnace and cast in argon atmosphere, U.P.B. Sci. Bull., Series B, Vol. **86**, Iss. 2, 2024.

[9] *K. Park, P. Withey*, Compositions of Gamma and Gamma Prime Phases in an As-Cast Nickel-Based Single Crystal Superalloy Turbine Blade, *Crystals*, Vol. **12**, Iss. 2, 2022.
[10] *P. Peng, L. Lu, Z. Liu, Y. Xu, X. Zhang, Z. Ma, H. Zhang, M. Guo, L. Liu*, Investigation on influence of Ta on microstructure evolution of directionally solidified Ni-based superalloys, J. Alloy Compd., Vol. **927**, 2022.
[11] *Y. Amouyal, Z. Mao, D. N. Seidman*, Effects of tantalum on the partitioning of tungsten between the γ- and γ′-phases in nickel-based superalloys: Linking experimental and computational approaches, Acta Mater., Vol. **58**, Iss. 18, 2010.
[12] *M. Huang, Y. Ma, Y. Wu, W. Zheng, M. J. Pavel, M. L. Weaver, W. Meng, Y. Long, S. Ngai, X. Wang, P. Zhang, W. Li, F. Vogel*, Effect of γ forming element additions on the homogenization behavior and formation of hierarchical microstructures in Ni-based superalloys, J. Alloy Compd., Vol. **975**, 2024.
[13] *Z. Qin, W. Li, Z. Wang, J. Pan, Z. Wang, Z. Li, G. Wang, J. Pan, F. Liu, L. Huang, L. Tan, L. Zhang, H. Han, H. Chen, L. Jiang*, High - throughput characterization methods for Ni-based superalloys and phase prediction via deep learning, J. Mater. Res. Technol., Vol. **21**, 2022.
[14] *T. Brynk, Z. Pakiela, K. Ludwichowska, B. Romelczyk, R. M. Molak, M. Plocinska, J. Kurzac, T. Kurzynowski, E. Chlebus*, Fatigue crack growth rate and tensile strength of Re modified Inconel 718 produced by means of selective laser melting, Mat Sci Eng A-Struct, Vol. **698**, 2017.
[15] *A. Mottura, R. Reed*, What is the role of rhenium in single crystal superalloys ?, MATEC Web of Conferences, Vol. **14**, 2014, EUROSUPERALLOYS 2014 – 2nd European Symposium on Superalloys and their Applications, https://doi.org/10.1051/matecconf/20141401001
[16] *X. Wu, S.K. Makineni, C.H. Liebscheret al.*, Unveiling the Re effect in Ni-based single crystal superalloys, Nat. Commun., Vol. **11**, 2020.
[17] *V. Kindrachuk, N. Wanderka, J. Banhart, D. Mukherji, D. Del Genovese, J. Rösler*, Effect of rhenium addition on the microstructure of the superalloy Inconel 706, Acta Mater, Vol. **56**, Iss. 7, 2008.
[18] *Y. Cheng, X. Zhao, W. Xia, Q. Yue, Y. Gu, Z. Zhang*, The overview of the formation mechanisms of topologically close-packed phases in Ni-based single crystal superalloys, Mater Design, Vol. **237**, 2024.
[19] C.M.F. Rae, M.S.A. Karunaratne, C.J. Small, R.W. Broomfield, C.N. Jones, R.C. Reed, Topologically Close Packed Phases InAn Experimental Rhenium-Containing Single Crystal Superalloy, Superalloys 2000 Edited by T.M. Pollock et al, TMS (The Minerals, Metals & Materials Society), 2000.
[20] *Sims, C. T., Stoloff, N. S., Hagel, W. C.*, Superalloys II, Wiley, New York, 1986.
[21] *X. Liu, J. Fan, P. Zhang, K. Cao, Z. Wang, F. Chen, D. Liu, B. Tang, H. Kou, J. Li*, Influence of heat treatment on Inconel 625 superalloy sheet: carbides, γ″, δ phase precipitation and tensile deformation behaviour, J. Alloy Compd., Vol. **930**, 2023.
[22] *D. Deng, R.L. Peng, H. Brodin, J. Moverare*, Microstructure and mechanical properties of inconel 718 produced by selective laser melting: Sample orientation dependence and effects of post heat treatments, Mat Sci Eng A-Struct, Vol. **713**, 2018.
[23] *D. Ivanov, A. Travyanov, P. Petrovskiy, V. Cheverikin, E. Alekseeva, A. Khvan, I. Logachev*, Evolution of structure and properties of the nickel-based alloy EP718 after the SLM growth and after different types of heat and mechanical treatment, Additive Manufacturing, Vol. **18**, 2017.